Journal of Applied Fluid Mechanics, Vol. 13, No. 1, pp. 233-243, 2020.
Available online at www.jafmonline.net, ISSN 1735-3572, EISSN 1735-3645.
DOI: 10.29252/jafm.13.01.30148

Effect of Air Quantity Distribution Ratio on Flame Height of Flue Gas Self-Circulation Burner

K. Xie[1†], Y. J. Cui[2], X. Q. Qiu[1] and J. X. Wang[3]

[1] *College of Chemical Engineering, China University of Petroleum (East China), Qingdao, 266580, China*
[2] *College of Electromechanical Engineering, China University of Petroleum (East China), Qingdao, 266580, China*
[3] *Research and Development Department, Yunnan Aerospace Industry Co. Ltd, Kunming, 605299, China*

†*Corresponding Author Email: xiekai199101@163.com*

(Received February 10, 2019; accepted April 9, 2019)

ABSTRACT

It is a difficult scientific problem of applied fluid mechanics that the flame is too long and does not match the furnace chamber in a small restricted heating space. This paper aims to investigate the effect of the air quantity distribution ratio on the flame height of a flue gas self-circulation burner. In order to obtain a better combustion emission effect and a shorter flame height, a burner head structure with a small flue gas self-circulation was designed. Numerical simulation was employed to investigate the effect of the different distributions of central air, swirling air and secondary air on flame height. The periodic boundary condition model was adopted and the numerical model was compared and validated by experiment. Correlation analysis was used to determine the influence of the air inlet ratio of each part on the flame height and recirculating flue gas ratio (RFGR). The results show that the influence of different air quantity distributions on flame length is very significant. A reasonable central air ratio is a necessary condition for the good combustion of this flue gas self-circulation burner. Secondary air can effectively increase the RFGR, and flame height was significantly shorter with the increase of RFGR, but when it increased to more than 12%, the flame length was basically no longer shortened. On the premise of stable combustion, when the ratio of central air, swirling air and secondary air are respectively 25%, 35% and 40%, the shortest flame length is achieved. This work reveals an influence mechanism of the flame height of a small burner with a flue gas circulation structure. These results can provide theoretical support and an engineering design basis for the short flame problem in a small restricted space.

Keywords: Air quantity distribution; Central air; Swirling air; Secondary air; RFGR; Flame height.

NOMENCLATURE

E	specific internal energy	Re	relative Reynolds number
f	average mixture fraction	$RFGR$	Recirculating Flue Gas Ratio
F_D	drag force of the droplet	T	local temperature
h	specific enthalpy	u	instantaneous velocity
k	turbulent kinetic energy	Y	fuel mass fraction
L	flame length	t_{ij}	viscous stress tensor
LES	Large Eddy Simulation		
p	pressure	α	spray cone angle
PDF	Probability Density Function	γ	swirl groove angle
r	air–fuel ratio	ε	turbulence dissipation rate
$RANS$	Reynolds Averaged Navier-Stokes Simulation	ρ	density
		σ	standard deviation

1. INTRODUCTION

Spray flame in small confined spaces is widely used in logistical stoves, small furnaces, emergency rescue square cabins and other chemical heat transfer process in the industrial process (Daho *et al.*, 2014). The required flame length is closely related to the limited space size. If a small combustion chamber has a long flame, the flame will directly flush the heating surface, resulting in

the sudden cooling of unburned oil mist or gas and carbon accumulation on the heating surface. If the combustion chamber is large and the flame is especially short, the phenomenon of poor flame saturation and low temperature will appear in the furnace, which will seriously affect the thermal utilization of the heating surface.

The fuel needs to be atomized before evaporative ignition, which belongs to vaporization combustion. There is no accurate theoretical formula to determine the flame length of the nozzle for forced air supply. The structure and temperature of a flame under different distribution ratios of a fuel burner were investigated (Qiu *et al.*, 2009). The study showed that the effect of secondary air can reduce the flame temperature and create an even mixture of oil mist and air evenly. Some studies (Xu *et al.*, 2012) have shown that the central air volume should not be too large, otherwise the formation of backflow area will be affected, thereby affecting the ignition position of fuel oil. The initial and secondary air of a 600 MW large-scale cyclone burner were studied (Zhou *et al.*, 2014). The results showed that the secondary air is more favorable for the high temperature area of the flame to move towards the nozzle, so the flame becomes shorter. Similar results were obtained in the study of air distribution in a propane burner (Liu *et al.*, 2015). A number of experiments have shown that a reasonable combination of primary air and secondary air has a very positive effect on the flame temperature in the furnace (Wu *et al.*, 2016). Some scholars have studied the adaptive air distribution by improving the nozzle structure and the results also showed that the organization of air flow is very important (Li et al., 2018; Elbaz and Roberts, 2016). Ling *et al.* (2015a and 2015b) investigated the location of flue gas self-circulation in a heavy oil swirl burner, and found that different flue gas reflux ratio had a great impact on the flame position, temperature and pollutant emission. Similar studies of large boiler swirl burners have shown that the flame height increases as the ratio of secondary air increases (Wang *et al.*, 2018). For the study of the air distribution of a slightly less powerful burner (900 kW), Luo *et al.* (2015) also believed that the reasonable secondary air ratio was beneficial to the increase of the combustion temperature. In smaller restricted spaces, the required burner power is usually less than 100 kW. It is difficult to adjust the flame length for small power burners with a flue gas self-circulation structure. For fuel injection burners, in addition to good atomization conditions, only the accurate regulation of distribution proportion ensures the best airflow structure to form a flame that is best adapted to small restricted spaces.

The current research shows that the adjustment of flame length can be achieved by proper air distribution (Savard *et al.*, 2018). Although many scholars have made significant contributions to the relationship between air distribution and combustion, these are mainly concentrated in large and high-power industrial combustion devices. There is not a very deep understanding of the influence of the air quantity distribution ratio on flame height. We aim to determine the ratio that can keep the flame stable and the ratio that should be employed when the shortest flame possible is needed in a small structure. In addition, there is no definite answer as to whether the recirculating flue gas ratio (RFGR) plays a decisive role in regulating the flame length of a low-power fuel burner with a flue gas self-circulation structure. Therefore, this paper focuses on the study of the air distribution ratio in a smaller power burner with a flue gas self-circulation structure. The effect of RFGR on flame length is also investigated. This research can play an important theoretical guiding role in the design of burners for small-scale furnaces and chemical heating equipment.

In the present work, first a combustion head structure with flue gas self-reflux structure is designed to reduce the emission of the pollutant NOx by flue gas self-circulation during combustion. Experiments show that NO emissions are relatively low when this structure is adopted, so this paper does not elaborate on the pollutant. In the process of swirl spray combustion, the air distribution pattern includes the following three types: central air, swirl air and secondary air. The optimal proportions of these three air intake forms is the focus of this research.

2. METHODOLOGY

2.1 Burner Modeling

Eldrainy *et al.* (2011) designed a structure with an adjustable air distributor for gas turbine burners, and the large eddy simulation results showed that the central flue gas backflow area is crucial to the stable flame. For the swirl spray jet in the restricted space of the furnace, in addition to the central vortex reflux region, an external reflux region is generated under the strong entrainment action of the outer boundary of the jet, thus forming two stable combustion heat sources in the central and peripheral reflux regions.

Figure 1 presents the structure diagram of the burner head with flue gas self-circulation. In the flue gas self-circulation burner, an outer cylinder with a 7.5 mm wide annular outlet is placed over the flame holder. Meanwhile, in order to enhance the ejection effect at the edge of the inner cylinder, a contraction structure replaces the previous exit. With this structural design, the negative pressure inside the inner cylinder increases with the enhanced of secondary air ejection, which can improve the reflux flow of the flue gas. The ratio of the flue gas flow through this opening to the total air flow is the RFGR.

Two air distribution devices both the prototype burner and new burner, feature a swirl flame holder with an opening groove at an angle of 45°, as shown in Fig. 2. The swirl slots are uniformly distributed in the range of 360°. The total length of the combustion chamber is 1150 mm, the bottom diameter is 500 mm, the flue gas outlet is 150 mm and the outlet diameter is 250 mm. In addition, the

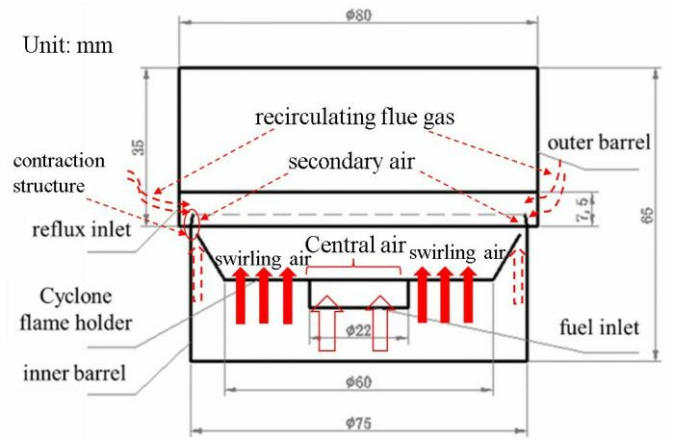

Fig. 1. Structure of the burner head with flue gas self-circulation.

periodic boundary condition model is used to reduce the calculation cost. Because of the symmetry of the burner head model and the combustion chamber, the model is one-fifth of the actual device. The combustor model is shown in Fig. 3.

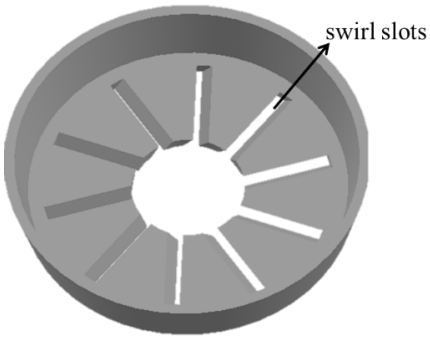

Fig. 2. Three-dimensional structural drawing of the flame holder.

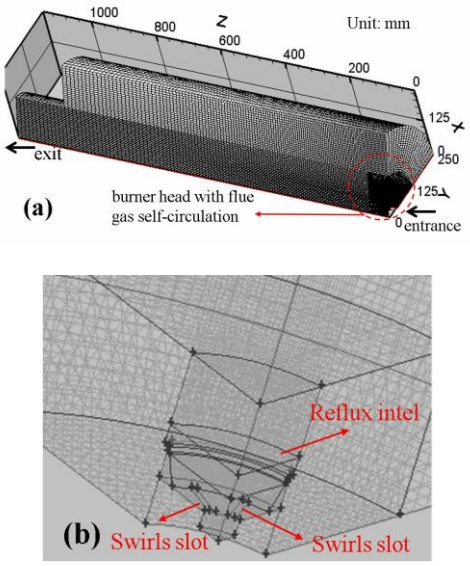

Fig. 3. Computation model of the meshing (a) Entire combustion chamber model, (b) burner head with flue gas self-circulation.

According to the actual situation of this model, the whole solution region is divided into several small regions. In the regular region, a structured grid is used, and in the small irregular region an unstructured grid is used. The number of grids in the final calculation model is 199,000, and the relevant grid independence verification is detailed in Section 3.1. The maximum skewness is 0.78, so the mesh quality is adequate.

2.2 Numerical Theory and Model

Numerical calculation has been widely used in combustion, and its calculation accuracy is comparable with experimental results, especially in engineering applications (Shi *et al.*, 2015; Alam *et al.*, 2019).

Kurreck *et al.* (1998) measured various flow characteristics and the temperature distribution in a three-dimensional stable jet combustor model using the standard *k-ε* model. They then compared their numerical simulation results with the measured data reported by Bauer *et al.* (1995) and verified the reliability of the model. The LES model is indeed much more accurate in the solution of vortices, but in the engineering application research of fluid structures, if the internal structure of the flame is not studied and the computational cost is taken into account, the RANS model is still the first choice. Yilmaz *et al.* (2017) studied different turbulence models of hydrogen-air flames, and the results showed that there was no significant difference in the simulation results of the two equation turbulence models (standard *k-ε*, renormalization group *k-ε*, realizable *k-ε*). The swirl intensity of the simulated combustion flow in this paper is not high, and the economic efficiency of the calculation is taken into account when there is no obvious difference in the results. In this paper, the *k-ε* turbulence model was selected. Earlier, Repp *et al.* (2002) studied the turbulence-chemical interaction in a closed swirl diffusion flame with the assumed Probability Density Function (PDF) model and found that the model fully met the engineering application requirements. Subsequently, some scholars (Jones *et al.*, 2012; Shum-Kivan *et al.*, 2017) used the PDF model to calculate the spray

combustion and obtained good prediction results of flame temperature and morphology.

In this paper, the standard *k-ε* turbulence model suitable for initial iteration, design selection, and parameter study was selected, and the droplet distribution and flow trajectory were predicted using Discrete Phase Modeling (DPM) coupled with a calculation method (Jenny *et al.*, 2012). The combustion model was simplified as a PDF model. The assumption of the whole numerical calculation is that the flame is stable and steady in the combustion chamber.

Fundamental Governing Equation. The gas phase control equation describing the three-position steady-state flow in the combustion chamber mainly includes the following (taking the x-direction as an example) (Datta and Som, 1999).

Mass conservation equation:

$$\frac{\partial \rho}{\partial t}+\frac{\partial}{\partial x_i}(\rho u_i)=0 \tag{1}$$

where ρ is the density and u_i is instantaneous velocity in the i direction.

Momentum conservation equation in the i direction (in the inertial (non-accelerating) coordinate system):

$$\frac{\partial}{\partial t}(\rho u_i)+\frac{\partial}{\partial x_j}\left(\rho u_i u_j\right)=-\frac{\partial p}{\partial x_i}+\frac{\partial \tau_{ij}}{\partial x_j}+\rho g_i+F_i \tag{2}$$

where τ_{ij} is the viscous stress tensor and F_i refers to the external volume force (such as the lift force generated by the interaction of discrete phases), which is not limited to a certain force and includes other related source terms of the model.

Species transport equation:

$$\frac{\partial}{\partial t}(\rho Y_i)+\nabla\left(\rho \vec{v} Y_i\right)=-\nabla \vec{J}_i+R_i+S \tag{3}$$

where Y is the mass fraction of the components, J_i is the diffusion of component i, R_i is the net rate of the chemical reaction for component i and S is the extra formation rate of the discrete phase and other source phases.

Energy conservation equation:

$$\frac{\partial}{\partial t}(\rho E)+\frac{\partial}{\partial x_i}\left[u_i\left(\rho E+p\right)\right]=\frac{\partial}{\partial x_i}\left[k_{eff}\frac{\partial T}{\partial x_i}-\sum_{j'}h_{j'}J_{j'}+u_j\left(\tau_{ij}\right)_{eff}\right]+S_h \tag{4}$$

where k_{eff} is the effective heat transfer coefficient, $J_{j'}$ is the diffusion flux of component j' and τ_{ij} is effective viscous stress tensor. The first three terms on the right-hand side of the Eq. (4) describe energy transport due to heat transfer, component diffusion, and viscous dissipation, respectively. S_h is the heat source term. It contains the heat of chemical reaction, the term of radiation source and heat transfer between continuous and discrete phases.

Turbulence Model. The turbulent kinetic energy and turbulent dissipation rate in the turbulence model are determined by the following two equations:

$$\frac{\partial}{\partial x}(\rho k \vec{v})=\frac{\partial}{\partial x}\left[(\mu+\frac{\mu_t}{\sigma_k})\frac{\partial k}{\partial x}\right]+G_k+G_b-\rho\varepsilon-Y_M+S_k \tag{5}$$

$$\frac{\partial}{\partial x}(\rho \varepsilon \vec{v})=\frac{\partial}{\partial x}\left[(\mu+\frac{\mu_t}{\sigma_\varepsilon})\frac{\partial \varepsilon}{\partial x}\right]+C_{1\varepsilon}\frac{\varepsilon}{k}(G_k+C_{3\varepsilon}G_b)-C_{2s}\rho\frac{\varepsilon^2}{k}+S_\varepsilon \tag{6}$$

where μ_t is the turbulence viscosity coefficient, determined by the following formula:

$$\mu_t=\rho C_\mu\frac{k^2}{\varepsilon} \tag{7}$$

where $C_{1\varepsilon}=1.44$, $C_{2\varepsilon}=1.92$, $C_\mu=0.09$, $\sigma_k=1.0$, $\sigma_\varepsilon=1.3$.

Discrete Phase Model. Due to the strong momentum, mass and energy transfer between the droplet and gas phases in the combustion reaction of discrete oil droplets, the coupling calculation method was adopted in this paper to predict droplet distribution and flow trajectory. The Lagrange method was used to track the motion and transport of the discrete droplets in the flow field (Fossi *et al.*, 2015). The particle inertia force equation is:

$$\frac{d\vec{v}_P}{dt}=F_D(\vec{v}-\vec{v}_P)+\frac{g(\rho_P-\rho)}{\rho_P}+F \tag{8}$$

where $\vec{v}$ is the continuous phase velocity, $\vec{v}_P$ is the particle phase velocity, g is the gravitational acceleration, and F is the additional force caused by the fluid pressure gradient in the flow field.

The drag force per unit mass of diesel droplet is:

$$F_D=\frac{18\mu}{\rho_P d_P^2}\frac{C_D Re}{24} \tag{9}$$

where C_D is the drag coefficient and Re is the relative Reynolds number. Equation (10) is the expression of Re.

$$Re=\frac{\rho d(\vec{v}-\vec{v}_P)}{\mu} \tag{10}$$

Considering the influence of turbulence on the randomness of particles, this paper adopted the random orbit model. In this model, the influence of instantaneous velocity on particle orbit is considered by random method. By calculating particle orbits enough times, the momentum, mass flux and other parameters defined by the jet source are evenly distributed across each particle orbit.

Radiation Model. For the combustion process with a two-phase coupling problem, the influence of discrete second-phase particles (such as carbon black particles generated by high-temperature and low-oxygen combustion) needs to be considered. The discrete ordinates radiation model (DO model) was applied in this paper, which is applicable to media of any optical thickness. The radiation intensity transfer equation in the space coordinate system is as follows:

$$\frac{dI(\vec{r},\vec{s})}{ds}+(a+\sigma_s)I(\vec{r},\vec{s})=an^2\frac{\sigma T^4}{\pi}+\frac{\sigma_s}{4\pi}\int_0^{4\pi}I(\vec{r},\vec{s}')\Phi(\vec{s},\vec{s}')d\Omega' \tag{11}$$

where α is the absorption coefficient, n is the refraction coefficient, σ_s is the scattering coefficient, σ *is* the Stefan–Boltzman constant, $\vec{r}$ represents the position vector, $\vec{s}$ is the direction vector, and $\vec{s}'$ is the scattering direction vector.

Combustion Model. Light diesel is a high-chain alkane mixture fuel composed of $C_{10}H_{20}$ to $C_{15}H_{28}$, etc. In terms of the hydrocarbon mass ratio, the combustion characteristics and equivalent mixing fraction of $C_{12}H_{23}$ are close to those of light diesel. Consequently, the light diesel component was simplified as a single component $C_{12}H_{23}$ (Klančišar *et al.*, 2016).

The combustion calculation based on a non-premixed combustion equilibrium chemical reaction was carried out in this paper. According to the chemical reaction mechanism of high-chain alkanes, and considering the existence of intermediate products, it is assumed that the reaction process consists of 21 components: N_2, O_2, $C_{12}H_{23}$(g), CHO, CO, CO_2, H, H_2, H_2O, HCO, O, OH, HO_2, HONO, H_2O_2, C_2H_6, CH_4, HCOOH, HOCO, O_3, c<s>. Here, g represents gas and s is solid. CO, H_2, OH, H, O, C (s) and so on are products of high-temperature dissociation.

Flame height is the focus of this paper. Here we calculate the chemical equivalent mixing fraction to define the flame front. Based on mole chemical equivalents, the chemical equation can be written as:

$$C_{12}H_{23}+71/4(O_2+3.76N_2)\rightarrow 12CO_2+23/2H_2O+66.74N_2 \tag{12}$$

The mass flow rate of light oil is 2.6 kg/h. According to the calculation of chemical mass conservation, the oxygen consumed is 8.84 kg/h, and the theoretical air consumed is 37.92 kg/h. So, the equivalent air–fuel ratio is calculated as:

$$r=\frac{m_{air}}{m_{fuel}}=\frac{37.92}{2.6}=14.58 \tag{13}$$

where, m_{air} is the mass of air consumed in theory and m_{fuel} is the mass of fuel.

The chemical equivalent mixed fraction is calculated as:

$$f_s=\frac{\varphi}{\phi+r}=\frac{1}{1+14.58}=0.064 \tag{14}$$

Flame length was defined according to the stoichiometric fraction, then the average mixture fraction of f between 0.064 and 1 represented the flame. The height in the contour of the mean mixture fraction is the flame length.

The whole calculation was conducted by the finite volume method. In order to ensure the reliability of the calculation results, the "PESTRO!" (Pressure Staggering Option) format was applied to the pressure item of spatial discretization. In addition, in all transport equations, a second-order upwind precision calculation was adopted for space derivatives of the advection terms and a SIMPLE (Semi-Implicit Method for Pressure Linked Equations) algorithm was used to solve the pressure–velocity coupling. The continuous phase was predicted by a Eulerian formulation, and the discrete liquid phase was tracked by a Lagrangian formulation. The gas phase data calculated by the Eulerian method and the particle data of the discrete phase interacted with each other, and the trajectory of the droplet was finally obtained by interactive calculation. In addition, the source term in the energy equation was an important link connecting the whole radiation, discrete phase and combustion components. All calculations were done in ANSYS FLUENT.

2.3 Scheme for Numerical Calculation

In this paper, the original burner without a flue gas self-circulation structure was numerically calculated, and the feasibility of the numerical model was verified by comparing the numerical calculation and experimental results. The air distribution ratio parameters of this experiment and numerical calculation are shown in Table 1. In addition, the new burner with flue gas self-circulation structure was designed in this paper for numerical calculation, in which the proportion of central air was 15%~45%, the swirling air was 15%~40%, and the proportion of secondary air was 25%~50%. The selection of these air ratio calculation ranges is based on the combination of various air ratio ranges of the prototype burner and the actual numerical calculation results. To ensure that the minimum ignition of a central air ratio and non-extinguishing secondary air ratio. The following Table 2 is the specific simulation experiment design table. In all the experiments, the spray cone angle is 60° and the swirl groove angle of the flame holder is 45°.

Table 1 Scheme for numerical calculation of prototype burner

Cases	Air quantity distribution ratio (%)		
	Central air	Swirling air	Secondary air
0	31.39	28.32	40.29

Table 2 Scheme for numerical calculation of flue gas self-circulation burner

Cases	Air quantity distribution ratio (%)		
	Central air	Swirling air	Secondary air
1	25	25	50
2	25	30	45
3	27	33	40
4	30	30	40
5	30	35	35
6	30	40	30
7	33	27	40
8	35	25	40
9	35	30	35
10	35	35	30
11	40	20	40
12	40	25	35
13	40	30	30
14	45	15	40
15	45	30	25

3. RESULTS AND DISCUSSION

3.1 Model and Mesh Independence Validation

The simulation results of temperature field and flame length of the prototype are respectively shown in Figs. 4 and 5. Compared with the results of simulation and experiment (Li, 2012), both of them have primary and secondary reaction zones and the corresponding positions and distribution laws are basically found to be consistent.

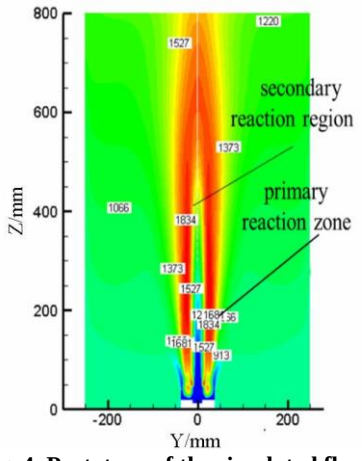

Fig. 4. Prototype of the simulated flame temperature field.

The maximum temperature of the simulated flame was 1834 K, and the maximum value of the experiment was 1810 K. Although the temperatures differed slightly, the corresponding position was consistent. The error was within the allowable range. In addition, the flame length fluctuated around 460 mm during the experiment, while the simulation results are 483 mm. In the calculation model, the depth of combustion head into combustion cylinder was 42mm; the value of 483mm was obtained by subtracting 42 from the actual scale size of 525 mm. The error between the two methods was less than 5%. Therefore, the simulation results were basically consistent with the experimental values within the error range. In conclusion, the applicability of the model was verified.

For numerical simulations, the appropriate mesh amount is equally important. The influence of the mesh size on the flame length was investigated by inspecting different mesh sizes within the range of 105,000~380,000 cells. Figure 6 confirms the independence of the present results in terms of flame height and maximum flame temperature from the mesh size. As can be seen from the figure, when the mesh cells were between 196,000 and 380,000, the flame length and the average temperature of the flame tended to be stable. Combined with the economy of the calculation time, the mesh of 190,000 cells was regarded as the optimum. This optimal mesh number was used throughout the present work.

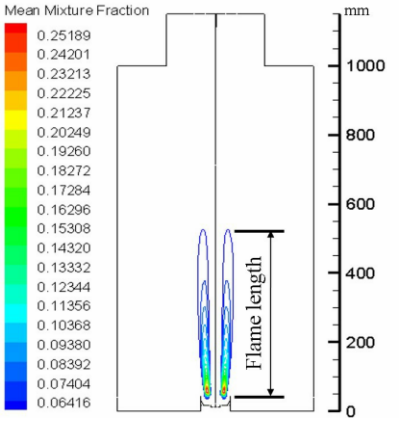

Fig. 5. Simulated contour of the mean mixture fraction (f = 0.06416~1).

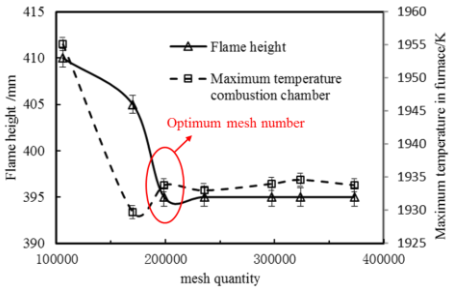

Fig. 6. Independence of the present solution from the mesh size: flame height and flame temperature.

3.2 Correlation Analysis of Air Distribution Ratio and Flame Length

The data of flame length and reflux ratio under different air distribution ratios were obtained according to experimental cases 1–15, as shown in Table 3.

Table 3 Flame length and recirculation ratio datasheet

Cases	Flame length (mm)	RFGR (%)
1	655	18.71
2	635	16.88
3	655	14.79
4	615	14.87
5	625	11.76
6	535	8.88
7	425	15.00
8	375	14.88
9	435	13.16
10	465	10.13
11	385	15.62
12	405	13.61
13	425	11.20
14	395	15.07
15	475	9.56

In the correlation analysis table, the two asterisks represent the correlation at the level of 0.01. One asterisk indicates correlation at the 0.05 level. Of course, the correlation is stronger at the 0.01 level. In the analysis in Table 4, the central air and flame length were significantly correlated at the level of 0.01, and the swirling air and flame length were significantly correlated at the level of 0.05. The influence of central air on RFGR was not so important. Both the correlation between secondary air and RFGR and the correlation between swirling air and RFGR were significant at the level of 0.01, and the correlation between secondary air and swirl air was as high as 0.966.

It can be seen that, as the air quantity distribution ratio has a greater impact on the flame length, and the central air is significantly correlated with the flame length, good combustion can be ensured in the initial oil and air mixture. Otherwise, the phenomenon of oil mist hitting the wall will occur or the device will be unable to burn. A good central air ratio is the first necessity to maintain good combustion. Increasing the proportion of central air can enhance the intensity of spray combustion at the nozzle outlet and shorten the flame. Moreover, it was found that the flame length of experiments 1 to 5 was too long without good central air conditions. Therefore, the correlation analysis was carried out from experiment 6 to experiment 15 with better central air conditions, as shown in Table 5.

As can be seen from Table 5, after ensuring a primary central air supply, swirling air had a significant correlation with flame length, with a value of 0.865 and a significant correlation at the level of 0.01. Secondary air also significantly correlated with flame length at the level of 0.01, with a value of 0.719. This indicates that swirling air plays a key role in determining the flame length. The influence of swirling air and secondary air on RFGR is more obvious, and this value increases from 0.609 to 0.844. After ensuring a good primary central supply of air, the swirling air, secondary air and RFGR were found to significantly correlate with the flame length. A certain amount of recirculating flue gas flow can shorten the length of the flame after ensuring a good initial mixing of central air and oil mist for stable combustion.

3.3 The Relationship Between Air Distribution Ratio and Flame Length

Firstly, the proportion of secondary air was analyzed. Figure 7 shows the flame length contour in different secondary air conditions. The relation between secondary air and flame length can be obtained as shown in Fig. 8. The outer edge of the flame showed an inward contraction with the increase of secondary air. This is mainly because with the increase of the proportion of secondary air, the proportions of central air and swirling air were lower. At this time, the effect of the axial momentum and radial momentum of the central air and the swirling air was obviously weaker than the ejection effect of the secondary air. Therefore, the increase of the proportion of secondary air caused the flame to shrink inward. Although secondary air can increase the RFGR, it should not be too large in the actual air quantity distribution. With the increase of secondary air, the flame length was first shortened. When secondary air contributed around 40%, the shortest flame was achieved, after which the flame length increased rapidly. This is mainly because the proper increase of the secondary air ratio enhanced the combustion rate of the initial flame area and made the flame shorter. However, once its ratio exceeded the critical value, it increased the instability of the flame, elongated the flame and eventually caused blow-off.

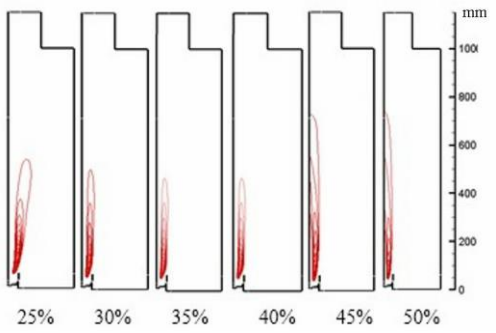

Fig. 7. Flame length contour with different secondary air ratios.

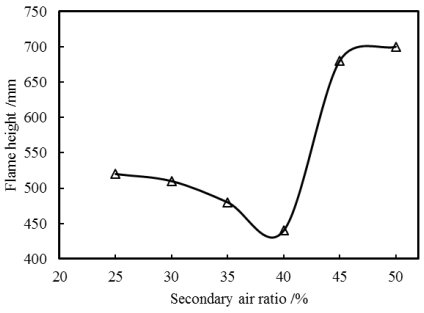

Fig. 8. The relation between flame length and secondary air ratio.

Table 4 Correlation analysis of experimental cases 1 to 15

Parameters		Central air	Swirling air	Secondary air	Flame length	RFGR
Central air	Pearson Correlation	1	−0.489 *	−0.549 *	−0.814 **	−0.375
	Significant (one-sided)		0.032	0.017	0.000	0.084
Swirling air	Pearson Correlation	−0.489 *	1	−0.460 *	0.487 *	−0.609 **
	Significant (one-sided)	0.032		0.042	0.033	0.008
Secondary air	Pearson Correlation	−0.549 *	−0.460 *	1	0.363	0.966 **
	Significant (one-sided)	0.017	0.042		0.092	0.000
Flame length	Pearson Correlation	−0.814 **	0.487 *	0.363	1	0.218
	Significant (one-sided)	0.000	0.033	0.092		0.218
RFGR	Pearson Correlation	−0.375	−0.609 **	0.966 **	0.218	1
	Significant (one-sided)	0.084	0.008	0.000	0.218	

Note: * Indicates significant correlation at the 0.05 level (one-sided); ** indicates a significant correlation at 0.01 level (one-sided)

Table 5 Correlation analysis of experimental cases 6 to 15

Parameters		Central air	Swirling air	Secondary air	Flame length	RFGR
Central air	Pearson Correlation	1	−0.638 *	−0.085	−0.440	0.158
	Significant (one-sided)		0.024	0.408	0.102	0.332
Swirling air	Pearson Correlation	−0.638 *	1	−0.713 *	0.865 **	−0.844 **
	Significant (one-sided)	0.024		0.010	0.001	0.001
Secondary air	Pearson Correlation	−0.085	−0.713 *	1	−0.719 **	0.948 **
	Significant (one-sided)	0.408	0.010		0.010	0.000
Flame length	Pearson Correlation	−0.440	0.865 **	−0.719 **	1	−0.872 **
	Significant (one-sided)	0.102	0.001	0.010		0.001
RFGR	Pearson Correlation	0.158	−0.844 **	0.948 **	−0.872 **	1
	Significant (one-sided)	0.332	0.001	0.000	0.001	

Note: * Indicates significant correlation at the 0.05 level (one-sided); ** indicates a significant correlation at the .01 level (one-sided)

When secondary air amounted to 40%, the ratio of central air and swirling air was correspondingly changed. The flame length contour is shown in Fig. 9. In this picture, we can intuitively see that both the central air and swirling air need to maintain reasonable and moderate proportions for the flame to maintained at a relatively short length. In addition, the relationship among swirl air, central air, and flame length can be obtained by an interpolation method, as shown in Fig. 10. It can be clearly seen from the figure that the flame is divided into three zones according to its length. The outer edge of the flame expands outward with the increase of central air. It is very necessary to maintain a certain central air quantity to ensure that the oil mist and air fully mix in the early stage. As the proportion of central air decreases, the flame length will be rapidly elongated. When both swirling air and central air are greater than 30%, an unstable flame area is created, resulting in excessive flame length, instability and even blow-off. The ratio that achieves the shortest flame length is around 35% central air and 25% swirling air. The central air of the flue gas self-circulation burner should not be less than 30%, otherwise, the flame will be quickly elongated and will not burn sufficiently. In addition, too small of a proportion of swirling air will inevitably lead to a larger axial momentum, in which is not easy to stabilize the flame, resulting in a longer flame and an outward expansion along the radial direction.

With the swirling air set to 30%, five groups of data were selected for the analysis of central air and secondary air. The flame length contour is shown in Fig. 11. The relationship among central air, secondary air and flame length is shown in Fig. 12. Consistent with the abovementioned observations, there were also three similar zones in terms of flame length. The obvious conclusion is that the difference between the proportion of central air and

secondary air should not too large. An unstable long flame area was created when central air amounted to less than 30% and secondary are amounted to more than 40%. This is mainly due to excessive secondary air, resulting in massive axial momentum at the exit of the burner cylinder edge. It is better to maintain the central air at around 35% under the structure of a flue gas self-circulation burner head. The proportion of secondary air at the point at which the shortest flame length was obtained was about 35% to 40%.

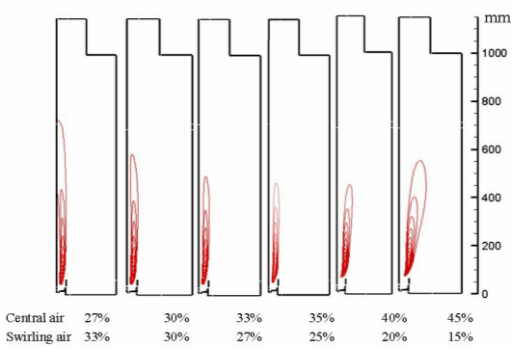

Fig. 9. Flame length contour with different swirling gas and central air ratios (secondary air 40%).

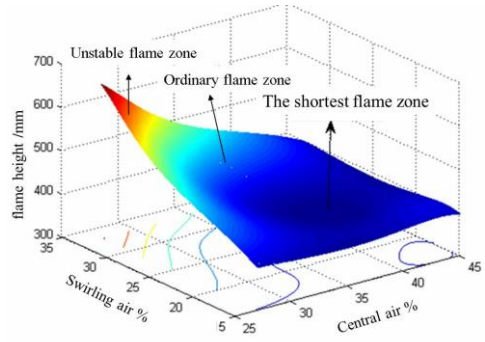

Fig. 10. Three-dimensional relationship of flame length with different swirling air and central air ratios.

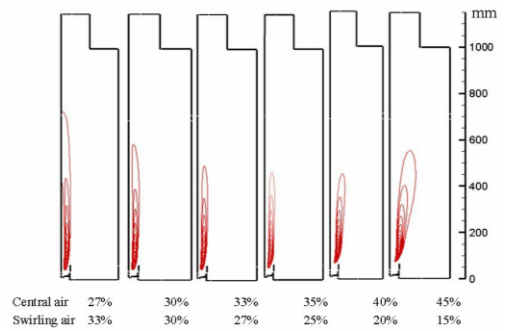

Fig. 11. Flame length with different central air and secondary air ratios (swirling air 30%).

3.4 The Relationship Between RFGR and Flame Length

According to the correlation analysis in Table 5, the correlation between RFGR and flame length was expressed at the level of 0.01. This is because after ensuring a good initial mixing of central air and oil mist for stable combustion, RFGR was found to be significantly correlated with flame length, and a moderate RFGR can thus shorten the flame length. The relationship between the flame length and RFGR is shown in Fig. 13.

First, we explain the unreasonable air distribution point in Fig. 13 after RFGR is greater than 12%. We used the difference of standard deviations between adjacent discrete data sets to analyze the dispersion of flame lengths in this interval (12<RFGR<16%). As a shorter flame length was the target, as we increased the value of RFGR, the flame length was calculated from the smallest to the largest, which are listed in Table 6. The equation for calculating the standard deviation here is as follows:

$$\sigma_n = \sqrt{\frac{1}{n}\sum_{i=1}^{n}\left(L_i - \bar{L}\right)^2} \tag{15}$$

where, L_i is the flame length of the i^{th} data and $\bar{L}$ is the average flame length from data 1 to data n.

Obviously, when n=5, the value of $\sigma_n - \sigma_{n-1}$ suddenly increases, that is to say, the dispersion index of the whole data set increases after adding the fifth value, indicating that the air distribution corresponding to these two points is unreasonable.

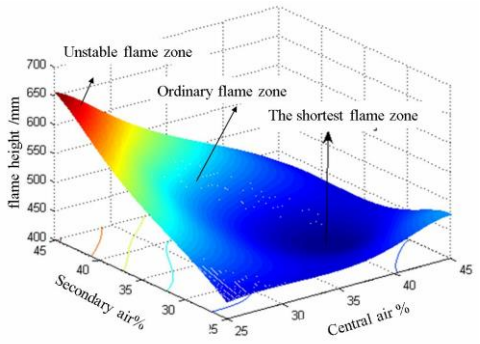

Fig. 12. Three-dimensional relationship of flame length with different central air and secondary air ratios.

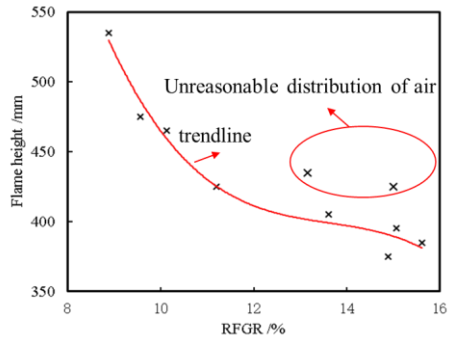

Fig. 13. The relation between flame length and RFGR.

Table 6 Dispersion index analysis using the standard deviation of flame length

n	Parameters		σ_n ($n\geq2$)	σ_n-σ_{n-1} ($n\geq3$)
	RFGR (%)	*L* (mm)		
1	14.88	375		
2	15.62	385	5	
3	15.07	395	8.16	3.16
4	13.61	405	11.18	3.02
5	15.00	425	17.20	6.02
6	13.16	435	21.15	3.94

When RFGR is relatively large, the mixing effect of oil mist and primary air will worsen, which is not conducive to combustion. Low-oxygen combustion will expand the flame volume and lengthen the flame. Therefore, a reasonable air quantity distribution ratio is particularly important. With the increase of RFGR, the flame length was obviously shortened, but after increasing to 12%, the curve tended to flatten. So, there is no need to increase RFGR blindly, as an overly large RFGR is ineffective.

4. CONCLUSION

In this paper, a flue gas self-circulation burner head structure was adopted, and the standard *k-ε* turbulence model, DPM, PDF, DO radiation models and periodic boundary conditions were applied in CFD calculations to simulate the flame of the burner in the closed combustion chamber. The results were compared and verified with the experiment. The influence of different proportion of central air, swirling air, secondary air and RFGR on flame height were investigated. The following conclusions were drawn:

(1) The effect of the air quantity distribution ratio on flame length is very significant. Under the structure of a flue gas self-circulation burner, a good central air ratio is the first necessary condition, and the primary air ratio should be kept at around 35%.

(2) The proportion of secondary air is reasonable at around 40%. To guarantee the flame stability, the swirling air should not be less than 20%. In this flue gas self-circulation burner, under the premise of ensuring flame stability, when the proportions of central, swirling and secondary air are 35%, 25%, and 40%, respectively, the flame length is the shortest as 385 mm, which is 15.4% lower than the length achieved with the original structure.

(3) The flame length becomes shorter as the RFGR increases (8.88%~15.62%), but an overly RFGR does not make the flame shorter. The optimum air quantity distribution ratio is especially important. In engineering applications, blindly pursuing a large RFGR is not an economic choice. Rather, a reasonable RFGR should be maintained.

ACKNOWLEDGEMENTS

This work was financially supported by the National Key R&D Program of China under Grant No. 2017YFC0806303.

REFERENCES

Alam, N., K. M. Pandey and K. K. Sharma (2019). Numerical investigation of combustion wave propagation in obstructed channel of pulse detonation engine using kerosene and butane fuels. *Journal of Applied Fluid Mechanics* 12(3), 883-890.

Bauer, H. J., L. Eigenmann, B. Scherrer and S. Wittig (1995). Local measurements in a three dimensional jet-stabilized model combustor. *ASME 1995 International Gas Turbine and Aeroengine Congress and Exposition, 5-8 June.*

Daho, T., G. Vaitilingom, O. Sanogo, S. K. Ouiminga, A. S. Zongo, B. Piriou and J. Koulidiati (2014). Combustion of vegetable oils under optimized conditions of atomization and granulometry in a modified fuel oil burner. *Fuel* 118, 329-334.

Datta, A. and S. K. Som (1999). Combustion and emission characteristics in a gas turbine combustor at different pressure and swirl conditions. *Applied Thermal Engineering* 19(9), 949-967.

Elbaz, A. M. and W. L. Roberts (2016). Investigation of the effects of quarl and initial conditions on swirling non-premixed methane flames: Flow field, temperature, and species distributions. *Fuel* 169, 120-134.

Eldrainy, Y. A., K. M. Saqr, H. S. Aly, T. M. Lazim and M. N. M. Jaafar (2011). Large eddy simulation and preliminary modeling of the flow downstream a variable geometry swirler for gas turbine combustors. *International Communications in Heat and Mass Transfer* 38(8), 1104-1109.

Fossi, A., A. DeChamplain and B. Akih-Kumgeh (2015). Unsteady RANS and scale adaptive simulations of a turbulent spray flame in a swirled-stabilized gas turbine model combustor using tabulated chemistry. *International Journal of Numerical Methods for Heat & Fluid Flow* 25(5), 1064-1088.

Jenny, P., D. Roekaerts and N. Beishuizen (2012). Modeling of turbulent dilute spray combustion. *Progress in Energy and Combustion Science* 38(6), 846-887.

Jones, W. P., S. Lyra, and S. Navarro-Martinez (2012). Numerical investigation of swirling kerosene spray flames using large eddy simulation. *Combustion and Flame* 159(4), 1539-1561.

Klančišar, M., T. Schloen, M. Hriberšek and N.

Samec (2016). Analysis of the effect of the swirl flow intensity on combustion characteristics in liquid fuel powered confined swirling flames. *Journal of Applied Fluid Mechanics* 9(5), 2359-2367.

Kurreck, M., M. Willmann and S. Wittig (1998). Prediction of the Three-Dimensional Reacting Two-Phase Flow Within a Jet-Stabilized Combustor. *Journal of Engineering for Gas Turbines and Power* 120(1), 77-83.

Li, D. P. (2012). *Research on combustion technology under extreme environmental conditions*. Ph.D. thesis, College of Chemical Engineering, China University of Petroleum, Qingdao, China.

Li, S., S. Zhang, L. Hou and Z. Ren (2018). Analysis of the Mixing and Emission Characteristics in a Model Combustor. *ASME Turbo Expo 2018: Turbomachinery Technical Conference and Exposition*, Oslo.

Ling, Z., H. Zhou and T. Ren (2015). Effect of the flue gas recirculation supply location on the heavy oil combustion and NOx emission characteristics within a pilot furnace fired by a swirl burner. *Energy* 91, 110-116.

Ling, Z., X. Zeng, T. Ren and H. Xu (2015). Establishing a low-NOx and high-burnout performance in a large-scale, deep-air-staging laboratory furnace fired by a heavy-oil swirl burner. *Applied Thermal Engineering* 79, 117-123.

Liu, C., S. Hui, S. Pan, D. Wang, T. Shang and L. Liang (2015). The influence of air distribution on gas-fired coal preheating method for NO emissions reduction. *Fuel* 139, 206-212.

Luo, R., J. Fu, N. Li, Y. Zhang and Q. Zhou (2015). Combined control of secondary air flaring angle of burner and air distribution for opposed-firing coal combustion. *Applied Thermal Engineering* 79, 44-53.

Qiu B. B., B. Y. Yang and W. Li (2009). Numerical simulation of the process of fuel combustion in the burner with different distribution of wind. *Journal of Anhui University of Technology (Natural Science)* 26(1), 5-8.

Repp, S., A. Sadiki, C. Schneider, A. Hinz, T. Landenfeld and J. Janicka (2002). Prediction of swirling confined diffusion flame with a Monte Carlo and a presumed-PDF-model. *International Journal of Heat and Mass Transfer* 45(6), 1271-1285.

Savard, B., H. Wang, A. Teodorczyk and E. R. Hawkes (2018). Low-temperature chemistry in n-heptane/air premixed turbulent flames. *Combustion and Flame* 196, 71-84.

Shi, J., J. Ran, C. Qin, M. Ran and L. Zhang (2015). Adaptive air distribution in an ejector burner for the utilisation of methanol-mixed fuels. *Fuel* 162, 313-322.

Shum-Kivan, F., J. M. Santiago, A. Verdier, E. Riber, B. Renou, G. Cabot and B. Cuenot (2017). Experimental and numerical analysis of a turbulent spray flame structure. *Proceedings of the Combustion Institute* 36(2), 2567-2575.

Wang, Q., Z. Chen, J. Wang, L. Zeng, X. Zhang, X. Li and Z. Li (2018). Effects of secondary air distribution in primary combustion zone on combustion and NOx emissions of a large-scale down-fired boiler with air staging. *Energy* 165, 399-410.

Wu, H., Z. Liu and H. Liao (2016). The study on the heat transfer characteristics of oxygen fuel combustion boiler. *Journal of Thermal Science* 25(5), 470-475.

Xu X. C., J. F. Lü and H. Zhang (2012). *Combustion theory and combustion equipment (The second edition)*. Science Press, Beijing, China.

Yıldırım, G. and Ş. Tokalıoğlu (2016). Heavy metal speciation in various grain sizes of industrially contaminated street dust using multivariate statistical analysis. *Ecotoxicology and environmental safety* 124, 369-376.

Yilmaz, H., O. Cam, S. Tangoz and I. Yilmaz (2017). Effect of different turbulence models on combustion and emission characteristics of hydrogen/air flames. *International Journal of Hydrogen Energy* 42(40), 25744-25755.

Zhou, H., Y. Yang, H. Liu and Q. Hang (2014). Numerical simulation of the combustion characteristics of a low NOx swirl burner: Influence of the primary air pipe. *Fuel* 130, 168-176.